THE UNIVERSITY of EDINBURGH

Edinburgh Research Explorer

Magnetic Disturbance Detection for Smartphone-based Indoor Positioning Systems with Unsupervised Learning

Citation for published version:
Dong, Y, Arslan, T & Yang, Y 2022, 'Magnetic Disturbance Detection for Smartphone-based Indoor Positioning Systems with Unsupervised Learning', *IEEE Transactions on Instrumentation and Measurement*, vol. 71, 2506411, pp. 1-1. https://doi.org/10.1109/TIM.2022.3163145

Digital Object Identifier (DOI):
10.1109/TIM.2022.3163145

Link:
Link to publication record in Edinburgh Research Explorer

Document Version:
Peer reviewed version

Published In:
IEEE Transactions on Instrumentation and Measurement

General rights
Copyright for the publications made accessible via the Edinburgh Research Explorer is retained by the author(s) and / or other copyright owners and it is a condition of accessing these publications that users recognise and abide by the legal requirements associated with these rights.

Take down policy
The University of Edinburgh has made every reasonable effort to ensure that Edinburgh Research Explorer content complies with UK legislation. If you believe that the public display of this file breaches copyright please contact openaccess@ed.ac.uk providing details, and we will remove access to the work immediately and investigate your claim.

Download date: 25. Apr. 2024

Magnetic Disturbance Detection for Smartphone-based Indoor Positioning Systems with Unsupervised Learning

Yinhuan Dong, Tughrul Arslan, *Senior Member, IEEE*, Yunjie Yang, *Member, IEEE*

***Abstract*—The smartphone magnetometer has been used in many indoor positioning systems to provide location information, such as orientation, user trajectory construction, and magnetic field-based fingerprint. However, suffering from magnetic disturbance, the magnetometer measurements are vulnerable to interference from metal infrastructures, electrical equipment, and other electronic devices in complex indoor environments. This paper extracts and explores the statistical features of the smartphone magnetometer measurements. Extensive experiments in various conditions show that the covariance and the magnitude difference can help detect the magnetic disturbance. Based on this, two unsupervised learning-based methods using Gaussian Mixture Model and k-means are developed to explore the two features mentioned above in magnetic disturbance detection. Experimental results demonstrate that the two proposed approaches have superior detection accuracy, which is 5% to 20% higher than the widely adopted vector selection methods in the literature.**

***Index Terms*—Indoor positioning system, smartphone, magnetometer, magnetic disturbance, unsupervised learning, clustering.**

I. Introduction

Nowadays, Location-Based Services (LBS) have played a vital role in our daily lives. They provide many user-centered applications in various contexts, such as work, entertainment, health, and personal life. Since the LBS industry's key requirement is accurate position information, positioning has gained significant interest in recent years. The Global Positioning System (GPS) and its variations could provide meter-level accuracy in many outdoor positioning scenarios [1]. Nevertheless, GPS accuracy is considerably limited by the walls, roofs, and other obstacles in complex indoor environments. Moreover, people spend much more time indoors than before, and 80% to 90% of our time is spent indoors [2]. Therefore, indoor positioning has become an attractive research area.

During the last decade, the wide expansion of smartphones brought a surge in new applications and services. Meanwhile, a variety of sensors built into modern smartphones show great potential to provide location information. For instance, the combination of inertial sensors, such as accelerometer, magnetometer, and gyroscope, enables the construction of user traces and trajectories while walking in indoor environments. The widespread usage of smartphone sensors makes the smartphone an excellent carrier to perform indoor positioning tasks. A number of indoor positioning technologies have been proposed, such as WiFi [3], radio frequency identification (RFID) [4], pedestrian dead reckoning (PDR) [5] and magnetic field [6].

The magnetometer is a sensor that measures the magnetic field intensity at a given point. It has been widely employed in many indoor positioning systems. These systems are grouped as magnetic field-dominated and magnetic field-aided approaches. On the one hand, a large body of works in the magnetic field-dominated approaches used magnetic field data to perform positioning tasks owing to its simplicity and ease of adaptation [7]. Most of such works like [8]–[10] follow the fingerprinting method, which estimates the user position by comparing the user collected data to the pre-recorded fingerprints (composed of magnetic field) annotated with known locations. These approaches could provide point-level and room-level positioning accuracy [11]. On the other hand, the magnetic field-aided approaches usually convert the measured earth magnetic field strength to Euler angle for user motion detection. A typical application is an electronic compass that integrates the accelerometer and magnetometer to determine the user heading relevant to the earth frame. Electronic compass has been implemented in many crowdsourced indoor positioning systems, such as in [12]–[14] to construct the user trajectory and annotate the trajectory with fingerprints (WiFi, Bluetooth, and other radio frequency signals). Therefore, magnetic field-dominated and magnetic field-aided approaches rely highly on the magnetic field's accurate measurement.

However, the magnetic field data measured by the smartphone magnetometer is vulnerable to hard-iron and soft-iron magnetic distortions [15]. In complex indoor environments, the magnetometer measurements are easily interfered with by metal infrastructures, electrical equipment, and other electronic devices, which results in severe error, particularly in magnetic field-aided approaches. Interfered magnetometer measurements are detrimental to the user heading estimation, consequently the user trajectory construction and the positioning accuracy. Some methods attempted to detect the magnetic disturbance by assuming a specific model of the magnetic disturbance. For example, Roetenberg *et al* [22] first proposed to model the magnetic disturbance as a first order Markov process. Some indoor positioning systems like [23] and [24] proposed in recent years have adopted such a method. Nevertheless, these model-based

The authors are with the School of Engineering, University of Edinburgh, Edinburgh, EH8 9YL, UK (e-mail: yinhuan.dong@ed.ac.uk; tughrul.arslan@ed.ac.uk; y.yang@ed.ac.uk).

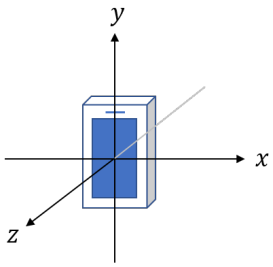

Fig. 1. Coordinate system relative to the smartphone.

TABLE I
NUMBER OF SAMPLES IN EACH SET

Dataset	Pure samples	Interfered samples	Total
SET 1	5970	5404	11374
SET 2	3161	3396	6557
SET 3	3287	3044	6331
SET 4	3672	2725	6397
SET 5	2345	2341	4686
SET 6	5562	5144	10706

methods are not resilient enough to the complex magnetic disturbance. Significant errors will occur if the disturbance does not obey the presupposed model [16]. Compared to the model-based methods, the vector selection method (VSM) has been widely adopted by many works such as [17]–[20]. Without extra computation, VSM detects the magnetic disturbance by setting thresholds of magnitude, dip angle, or both of them. Although such methods are easy to implement with low computation complexity, it is challenging to detect magnetic disturbance among the unstable values close to the threshold [21].

Different from the literature, this paper explores the statistical features of the pure and interfered samples and proposes two novel unsupervised learning-based magnetic disturbance detection (MDD) methods for smartphone-based indoor positioning systems. The main contributions of this paper are as follows:

- To the best of the authors' knowledge, this study is the first to propose to employ unsupervised learning to detect magnetic disturbances for smartphone-based indoor positioning systems.
- This study extracts and explores the statistical features of the pure and interfered samples from a large number of magnetometer measurements in various settings and show their effectiveness in detecting magnetic disturbances.
- Based on the statistical features, two magnetic disturbance detection methods using unsupervised learning are developed. The proposed methods are evaluated in static and dynamic situations to show their reliability and robustness. The proposed method demonstrates superior performance under all experimental conditions compared with conventional methods.

II. MOTIVATION

A. Element of the Magnetometer Measurement

The magnetic field measured by the smartphone magnetometer has three components along the x, y and z axis as shown in Figure 1. For a group of samples, $\mathbf{M}_x$, $\mathbf{M}_y$, and $\mathbf{M}_z$ are used to denote all the measurements along each axis, respectively. So that one magnetometer measurement can be defined as a three-dimensional vector:

$$\mathbf{m}_j = \begin{bmatrix} m_{x,j} \\ m_{y,j} \\ m_{z,j} \end{bmatrix} \tag{1}$$

where $\mathbf{m}_j$ denotes the jth measurement; $m_{x,j}$, $m_{y,j}$ and $m_{z,j}$ represent the three magnetic field components in micro teslas (μT).

B. Problem Analysis

In indoor environments, the magnetic field strength is vital in providing location information such as user heading and geomagnetic fingerprint. The magnetic field strength is a 3-dimensional vector that most mobile wireless devices can obtain. However, magnetic field strength measurements are usually inaccurate due to the magnetic disturbance caused by metal infrastructures and other electronic devices in the complex indoor scenario. Therefore, we collected a large number of measurements of the magnetic field strength and conducted a preliminary analysis. In this paper, the measurements with/without disturbance are defined as pure/interfered samples.

Figure 2 shows a large amount of three-axis magnetic field strength measurements from different settings, including different orientations, attitudes, test smartphones, and interference sources (the details of the experiment settings can be found in Section IV-A). The size of each set is listed in Table I. The only difference between the pure and interfered samples in each set is whether the interference source is added/removed. It can be observed from the figure that the joint variability of the three-axis magnetic field strength in different conditions (pure/interfered) is distinct. The interfered samples usually show higher variation than the pure samples in each set.

For further analysis, the covariance matrix is first calculated according to the covariance between the samples along each axis through the following equation:

$$\mathbf{C} = \begin{pmatrix} \mathrm{cov}(\mathbf{M}_x, \mathbf{M}_x) & \mathrm{cov}(\mathbf{M}_x, \mathbf{M}_y) & \mathrm{cov}(\mathbf{M}_x, \mathbf{M}_z) \\ \mathrm{cov}(\mathbf{M}_y, \mathbf{M}_x) & \mathrm{cov}(\mathbf{M}_y, \mathbf{M}_y) & \mathrm{cov}(\mathbf{M}_y, \mathbf{M}_z) \\ \mathrm{cov}(\mathbf{M}_z, \mathbf{M}_x) & \mathrm{cov}(\mathbf{M}_z, \mathbf{M}_y) & \mathrm{cov}(\mathbf{M}_z, \mathbf{M}_z) \end{pmatrix} \tag{2}$$

then the $p-$norms ($p = 2$ in our study) of the diagonal variance in the covariance matrix is calculated by:

$$l_i^p = \|\mathbf{C}^{diag}\| \tag{3}$$

where $\mathbf{C}^{diag}$ can be expressed by:

$$\mathbf{C}^{diag} = [\mathrm{cov}(\mathbf{M}_x, \mathbf{M}_x), \mathrm{cov}(\mathbf{M}_Y, \mathbf{M}_Y), \mathrm{cov}(\mathbf{M}_Z, \mathbf{M}_Z)] \tag{4}$$

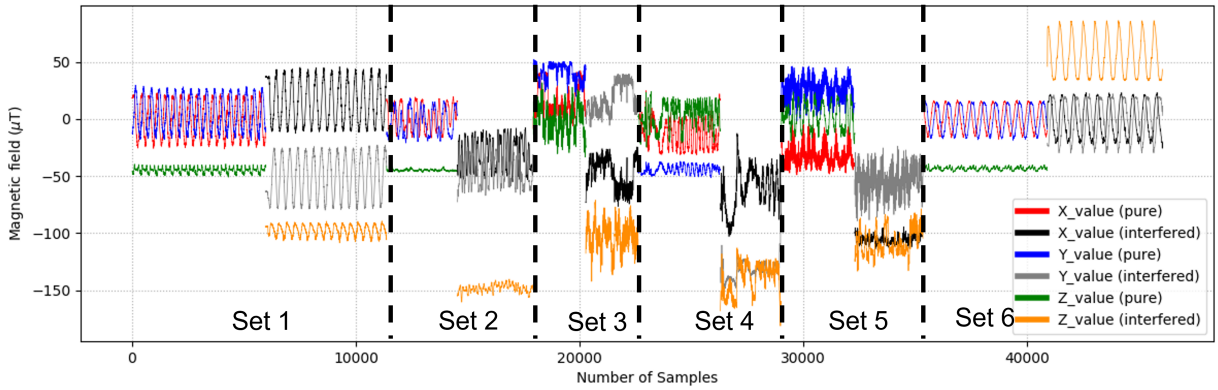

Fig. 2. A large amount of magnetic field strength measurements in different conditions. Each set stands for a collection with different settings.

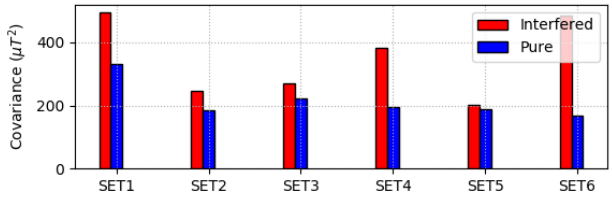

Fig. 3. Covariance of the interfered and pure samples in each set.

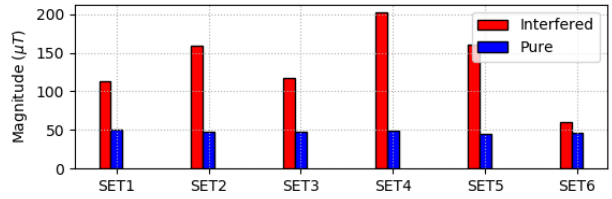

Fig. 4. Average magnitude of the interfered and pure samples in each set.

As the covariance norm l_i^p of pure and interfered samples are shown in Figure 3, it can be seen that the covariance of the interfered samples is usually higher than the pure samples in each set.

Besides, the average magnitude of the samples in each set is also calculated for comparison through the following equation:

$$\frac{1}{n}\sum_{j=1}^{n}|\mathbf{m}_j| \tag{5}$$

where the magnitude $|\mathbf{m}_j|$ is calculated by:

$$|\mathbf{m}_j| = \sqrt{(m_{x,j})^2 + (m_{y,j})^2 + (m_{z,j})^2} \tag{6}$$

As presented in Figure 4, it can be seen that the average magnitude of interfered samples is usually higher than the pure samples.

The above statistical analysis motivates us to develop algorithms to detect the magnetic disturbance utilizing the covariance and magnitude difference between the pure and interfered samples.

C. Problem Formulation

The first step of detecting magnetic disturbances is to automatically partition the dataset into two unlabeled clusters according to different statistical features (covariance/magnitude). Then, each cluster should be determined whether it is interfered or pure according to the characteristics of different features. The two steps are illustrated as follows:

- **Automatic Clustering:** Given a set of n test samples $\{\mathbf{m}_j\}^n$ where $\mathbf{m}_j$ is the jth measured magnetic field strength vector. As there should be only two clusters of pure and interfered samples in the entire dataset, the samples can be clustered by:

$$C_i = f(\mathbf{m}_j) \quad j = 1, 2, ...n \tag{7}$$

  where C_i denotes the ith ($i \in \{0, 1\}$) cluster, $f(\cdot)$ denotes the operation that divides the dataset into two clusters.
- **Empirical Labeling:** After obtaining two clusters of samples, it should be determined which cluster is most likely to be the representative of the interfered or pure samples:

$$L_i = g(C_i) \tag{8}$$

  where $L_i \in \{-1, 1\}$ is the label of the predicted cluster ($L = -1$ denotes that the cluster is interfered and $L = 1$ denotes that the cluster is pure); $g(\cdot)$ stands for the algorithm that developed to determine the label for each predicted cluster.

To solve the problems mentioned above, this study proposes two unsupervised learning-based magnetic disturbance detection (MDD) methods to partition the samples into two sets and determine the conditions of the predicted clusters. The details are discussed in the next section.

III. Unsupervised Learning-based Magnetic Disturbance Detection

This section details the key elements of the proposed methods to solve the magnetic disturbance detection problem. As the framework is shown in Figure 5, this paper develops and compares two unsupervised learning-based MDD methods using Gaussian Mixture Model and K-means. The two

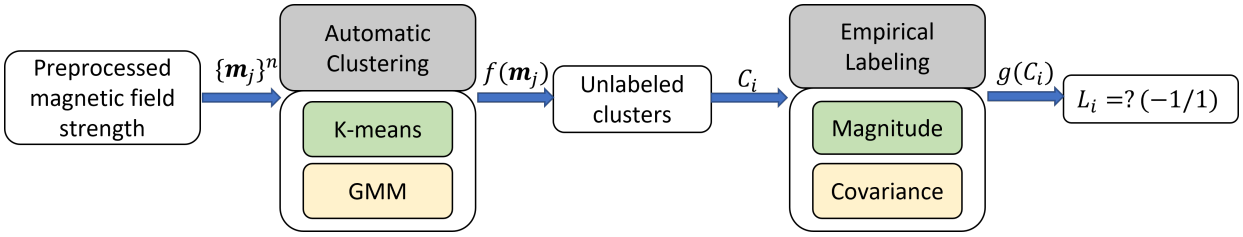

Fig. 5. The framework of the proposed MDD methods.

methods share the same pipeline with two main steps of Automatic Clustering and Empirical Labeling.

A. Preprocessing of Sensor Data

For each component of the magnetometer measurements, a filter is designed to smooth the data, which can be expressed by:

$$\mathbf{m}_j = \delta \mathbf{m}_{j-1} + (1-\delta)\mathbf{m}_j \tag{9}$$

where δ is the coefficient which can be expressed by:

$$\delta = \frac{\Delta t}{\Delta t + \frac{1}{f_c}} \tag{10}$$

where Δt denotes the sampling interval; f_c represents the cut-off frequency (7 Hz in our case).

B. Gaussian Mixture Model-based MDD Method

As mentioned above, the analysis shows that the three-axis magnetic field measurements' covariance could help identify whether the samples have interfered. Hence, the probability algorithm of Gaussian Mixture Model (GMM) is used to automatically partition the samples into two sets. Considering a dataset $\mathbf{M} \sim \{\mathbf{m}_1, \mathbf{m}_2, \ldots, \mathbf{m}_n\}$, a GMM can be regarded as an algorithm that generates k Gaussian models from $\mathbf{M}$. Expectation maximization (EM) algorithm is employed to get the model parameters and determine which model is most likely to generate each sample from the dataset. The samples generated from the same model will finally be clustered as one group.

A GMM is composed of a weighted sum of k component densities, which can be expressed by:

$$p(\mathbf{m}_j \mid \theta) = \sum_{i=1}^{k} \lambda_i p\left(\mathbf{m}_j \mid \boldsymbol{\mu}_i, \Sigma_i\right) \tag{11}$$

where λ_i is the coefficient ($\lambda_i \geq 0$); $p\left(\mathbf{m}_j \mid \boldsymbol{\mu}_i, \Sigma_i\right)$ represents the component Gaussian density that has a mean $\boldsymbol{\mu}_i$ and a covariance Σ_i, which can be expressed in the form of Gaussian function:

$$p\left(\mathbf{m}_j \mid \boldsymbol{\mu}_i, \Sigma_i\right) = \frac{1}{(2\pi)^{D/2}\left|\Sigma_i\right|^{1/2}} \times \exp\left\{-\frac{1}{2}\left(\mathbf{m}_j - \boldsymbol{\mu}_i\right)' \Sigma_i^{-1}\left(\mathbf{m}_j - \boldsymbol{\mu}_i\right)\right\} \tag{12}$$

the parameters of a complete GMM contains λ_i, $\boldsymbol{\mu}_i$ and Σ_i are collectively denoted by the notation θ.

The model parameters are estimated by maximizing likelihood estimation through the iteration of expectation-maximization (EM) algorithm [25]. According to $p(\mathbf{m}_j \mid \theta)$, the logarithmic likelihood function can be expressed by:

$$l(\theta) = \sum_{j=1}^{n} \log p(\mathbf{m}_j \mid \theta) \tag{13}$$

so that the parameter $\hat{\theta}$ can be computed by maximizing the logarithmic likelihood function:

$$\hat{\theta} = \arg\max l(\theta) \tag{14}$$

The iteration of EM algorithm first initializes the parameter θ, and then the parameter is replaced by a new estimated θ for the next iteration. Such a process is repeated until convergence. On each iteration, the parameters of the model are estimated by a posterior probability Pr_{ji} through the following formulas:

$$\hat{\lambda_i} = \frac{\sum_{j=1}^{n} \mathrm{Pr}_{ji}}{n} \tag{15}$$

$$\hat{\boldsymbol{\mu}}_i = \frac{\sum_{j=1}^{n} \mathrm{Pr}_{ji}\, \mathbf{m}_j}{\sum_{j=1}^{n} \mathrm{Pr}_{ji}} \tag{16}$$

$$\hat{\boldsymbol{\sigma}_i}^2 = \frac{\sum_{j=1}^{n} \mathrm{Pr}_{ji}\, \mathbf{m}_j^2}{\sum_{j=1}^{n} \mathrm{Pr}_{ji}} - \hat{\mu_i}^2 \tag{17}$$

where $\hat{\sigma_i}^2$ is the diagonal covariance; the posteriori probability Pr_{ji} $(j = 1, 2, ..., n, i = 1, 2, ..., k)$ is given by:

$$Pr_{ji} = \frac{\lambda_i p\left(\mathbf{m}_j \mid \boldsymbol{\mu}_i, \Sigma_i\right)}{\sum_{i=1}^{k} \lambda_i p\left(\mathbf{m}_j \mid \boldsymbol{\mu}_i, \Sigma_i\right)} \tag{18}$$

Now k ($k = 2$ in this study) components of Gaussian models are obtained which are responsible for modeling a group of samples from the dataset. Then, the probability of each sample $\mathbf{m}_j$ is calculated, which could be generated by the ith model by Equation 18:

$$P(\mathbf{m}_j) = [Pr_{1i}, Pr_{2i}, \ldots, Pr_{ki}] \tag{19}$$

where

$$\mathrm{Pr}_{ji} = \frac{\lambda_i p\left(\mathbf{m}_j \mid \boldsymbol{\mu}_i, \Sigma_i\right)}{\sum_{i=1}^{k} \lambda_i p\left(\mathbf{m}_j \mid \boldsymbol{\mu}_i, \Sigma_i\right)}, \sum_{i=1}^{k} \lambda_i = 1 \tag{20}$$

the samples are allocated to cluster C_i according to their highest probability $\hat{Pr}_{ji}$.

After then, the norm of the diagonal covariance of each mixture component is computed to determine which cluster is

interfered. Our analysis demonstrates that the covariance norm of interfered samples is larger than the pure samples caused by magnetic disturbance. Hence the samples are divided into two clusters by:

$$\mathbf{m}_j \in \begin{cases} C_1, & l_1^p \geq l_0^p \\ C_0, & l_1^p < l_0^p \end{cases} \tag{21}$$

where

$$l_i^p = \|\hat{\sigma_i}^2\| \tag{22}$$

so that the set with higher covariance (C_1) denotes the cluster of interfered samples ($L_1 = -1, L_0 = 1$). l_i^p is the norm of the ith component diagonal covariance ($p = 2$ in this study).

C. K-means-based MDD Method

In addition to the GMM-based MDD algorithm, this paper also proposes a k-means-based MDD algorithm to cluster the samples according to the difference in magnitude. K-means clustering is an unsupervised machine learning algorithm, which aims to find natural clusters for datasets according to the potentially similar patterns among individuals within the same cluster. For the dataset $\mathbf{M} \sim \{\mathbf{m}_1, \mathbf{m}_2, \ldots, \mathbf{m}_n\}$, the n samples are divided into $k(\leq n)$ clusters $C_i (i = 1, 2, \ldots, k)$. The principle of k-means clustering is to minimize the sum of squares of the divided clusters [26], which can be expressed by:

$$\arg\min_{\mathbf{M}} \sum_{i=1}^{k} \sum_{\mathbf{m}_j \in C_i} \|\mathbf{m}_j - \mathbf{c}_i\|^2, \quad j = 1, 2, ...n \tag{23}$$

where $\mathbf{c}_i$ is the mean value of the magnetic field strength in cluster C_i. To be more specific, the Euclidean distance can be expressed by the following function:

$$||\mathbf{m}_j - \mathbf{c}_i||^2 = \sqrt{(m_{x,j} - c_{x,i})^2 + (m_{y,j} - c_{y,i})^2 + (m_{z,j} - c_{z,i})^2} \tag{24}$$

Each training sample is allocated to its nearest neighbor centroid according to the Euclidean distance. After initialization, the new centroid for each cluster will be computed using the average of training samples in the corresponding cluster. The iteration of updating the centroid will stop once the Euclidean distance between the new and last centroid is less than the threshold.

In this study, as two conditions that the samples are collected with or without magnetic disturbance are considered, the number of predicted clusters k is set to 2. Therefore, the previous formula can be simplified to:

$$\arg\min_{\mathbf{M}} \sum_{i=1}^{2} \sum_{\mathbf{m}_j \in C_i} \|\mathbf{m}_j - \mathbf{c}_i\|^2, \quad j = 1, 2, ...n \tag{25}$$

After obtaining two sets of samples automatically partitioned by k-means, the two clusters are labeled according to the Euclidean distance from the centre of the cluster to the origin. The Euclidean distance can be calculated by:

$$d_i = \|\mathbf{c}_i - \mathbf{o}\|^2 \tag{26}$$

where c_j is the centroid (mean value) of the jth cluster; o is the coordinate of the origin $(0, 0, 0)$. According to our previous analysis, the cluster can be labeled by:

$$\mathbf{m}_i \in \begin{cases} C_1, & d_1 \geq d_0 \\ C_0, & d_1 < d_0 \end{cases} \tag{27}$$

so that has cluster C_1 with further Euclidean distance to the origin is labeled as interfered, while another one is pure ($L_1 = -1, L_0 = 1$).

IV. Experiments and Evaluations

This section presents the experiments set to analyze the magnetic disturbance detection problem and evaluate the performance of the proposed MDD methods.

A. Sites and Implementations

This subsection elaborates all eight experiments and eight different datasets in this study. Experiment 1 to Experiment 6 were set to collect a large number of magnetic field measurements from smartphones for our preliminary statistical analysis in Section II-B. Experiments 7 and 8 were set to test the performance of the proposed MDD methods. Different interference sources were used in the experiments to simulate real situations in people's lives. A metal box was used to simulate the interference from keys, metal accessories, or other metal components in people's bags and pockets. A smartphone was used to simulate the interference from electronic devices. And a heating radiator was used to simulate the magnetic disturbance from some infrastructures in indoor environments. All experiments were performed in open indoor environments away from crowd and obstacles/infrastructures unless specified.

Two different test phones are used in the experiments (see Figure 6). Both phones are integrated with the same magnetometer of AK09915. The location of the magnetometer in each phone is shown in Figure 7. The sensing range of this magnetometer is 4.7mT to 5.2mT.

For both pure and interfered samples in all experiments, the magnetometer measurements were read and recorded continuously with the sensor refresh rate of 50Hz. The smallest sampling interval of recording the magnetometer measurements was 0.04s.

1) Experiment 1 (SET1): In this experiment, a metal (iron) box was set as the interference. The perturbed samples were collected when test phone 1 was set in the box with the lid opened (as shown in Figure 8). In contrast, the pure samples were collected when the box was removed and away from other magnetic materials or structures. A digital rotating stand was used to simulate the heading direction changes of a user when the phone is held by the user horizontally. The digital rotating stand kept spinning clockwise at a speed of 3 rounds per minute when collecting samples.

2) Experiment 2-5 (SET2-5): These experiments were outdoors, away from any magnetic materials or structures on a different smartphone (test phone 2). An interference phone was used to create a magnetic disturbance in this experiment. The pure samples were collected when only test phone 2 was

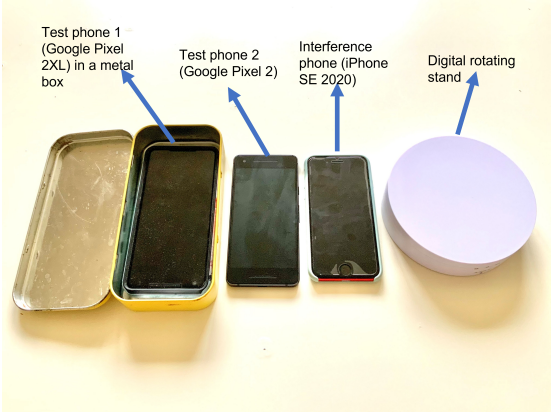

Fig. 6. Experimental devices: from left to right, test phone 1 (Google Pixel 2XL) in a metal box, test phone 2 (Google Pixel), interference phone (iPhone SE 2020) and a digital rotating stand.

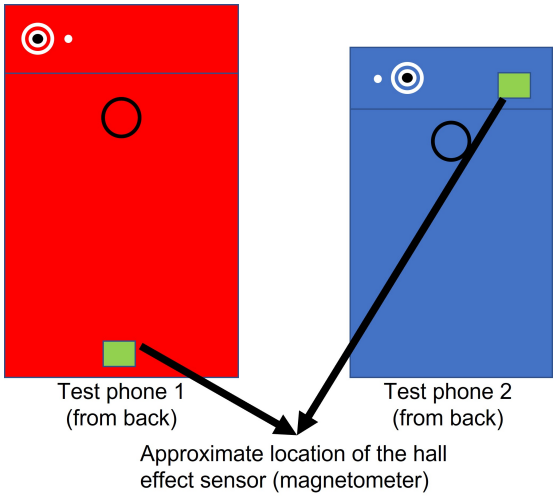

Fig. 7. The approximate location of the hall effect sensor (magnetometer): at the bottom of the motherboard of test phone 1; at the top of the motherboard of the test phone 2. Note that the actual size of the sensor is much smaller than the ones in the figure.

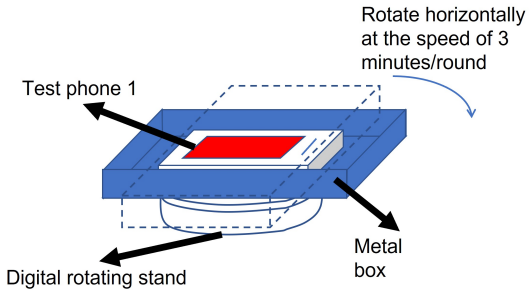

Fig. 8. Experimental settings of Experiment 1 for the preliminary analysis: test phone 1 is set in the metal box on the digital rotating stand to collect interfered data in Experiment 1.

with the volunteer, while the interfered samples were collected when the interference phone was attached to test phone 2. As the settings are shown in Figure 9, the volunteer was asked to take the phone(s) in different attitudes (Holding, Swing, Shirt Pocket, and Pant Pocket) and walked randomly as a pedestrian.

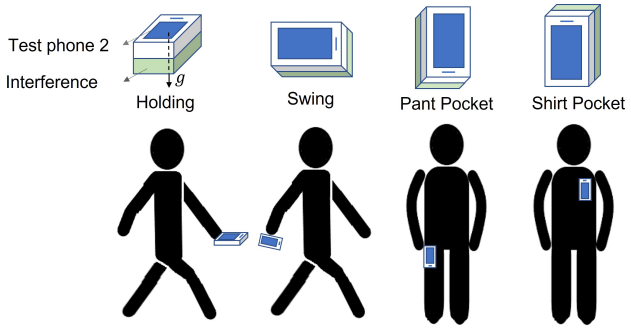

Fig. 9. Experimental settings of Experiment 2-5 for the preliminary analysis: the volunteer as asked to collect the interfered samples from test phone 2 in Experiment 2-5 in four different attitudes.

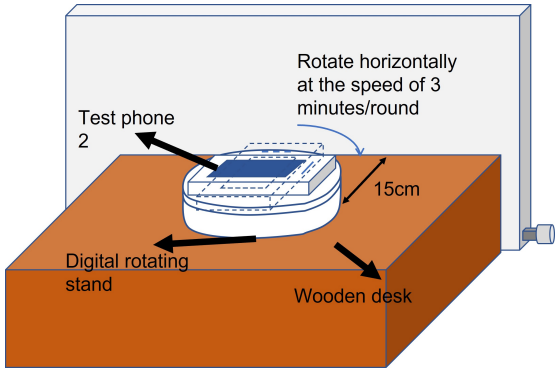

Fig. 10. Experimental settings of Experiment 6 for the preliminary analysis: test phone 2 is set on the digital rotating stand near a heating radiator to collect interfered samples for Experiment 6.

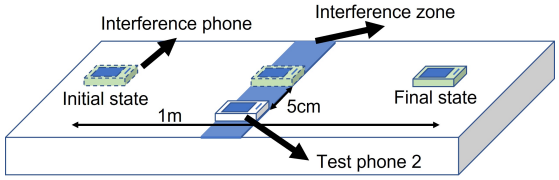

Fig. 11. Experimental settings of Experiment 7 for the static test: the interference phone was moved past the test phone 2.

The details of the four situations are illustrated below:

- **Holding (SET2)**: The smartphone is held horizontally by the volunteer.
- **Swing (SET3)**: The smartphone is held in hand and swung beside the volunteer's body.
- **Shirt Pocket (SET4)**: The smartphone is placed in the front shirt pocket of the volunteer.
- **Pant Pocket (SET5)**: The smartphone is placed in the front pant pocket.

3) Experiment 6 (SET6): In Experiment 6, the interference was again changed. Similar to Experiment 1, the smartphone was set on the digital rotating stand to collect samples. As shown in Figure 10, test phone 2 was placed near a heating radiator to collect interfered samples. In contrast, the pure samples were collected away from the heating radiator and other magnetic materials or structures.

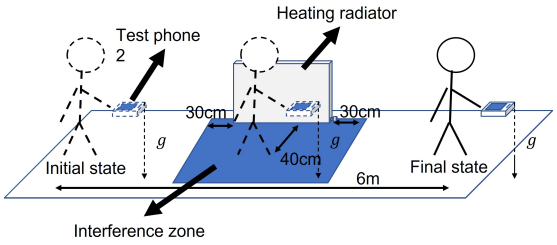

Fig. 12. Experimental settings of Experiment 8 for the dynamic test: the volunteer was asked to hold the test phone 2 and pass the heating radiator.

TABLE II
DETAILS OF THE DATASETS USED IN THE REAL TESTS

Test	Dataset	Interference duration	Pure samples	Interfered samples	Total
Static test	SET7	10s	338	252	590
Dynamic test	SET8	6.7s	393	169	562

4) Experiment 7 (SET7): This Experiment was set to evaluate the performance of the proposed MDD methods in the static mode. As the setting is shown in Figure 11, the samples were recorded while moving the interference phone slowly and pass the test phone 2. The test phone was fixed at a certain location. Note that both test and interference phones were set on a wooden desk horizontally. The measured samples were then labeled according to the time when test phone 2 was approaching/leaving the interference zone.

5) Experiment 8 (SET8): This Experiment was set to evaluate the performance of the proposed MDD methods in the dynamic mode considering a more critical condition. As the setting is shown in Figure 11, the samples were recorded while the volunteer was holding the test phone 2 and walking past the heating radiator. Similar to Experiment 7, the measured samples were then labeled according to the time when test phone 2 was approaching/leaving the interference zone.

B. Evaluation

This subsection evaluates the proposed methods by applying them to the samples collected in the experiments illustrated in the previous subsection. The details of the datasets used are shown in Table II. This study comprehensively evaluates the proposed methods from the following aspects:

- The disturbed samples are compared to the reference to show the detected distortions visually.
- Statistical features of the predicted samples/clusters are calculated and compared to the ground truth to verify the consistency of the proposed models.
- 3-D visualization of the samples with predicted and true labels are presented to further verify the proposed models.
- Detection accuracy is computed to quantify the performance of the proposed methods.
- A widely adopted vector selection method (VSM) [17]–[20] is implemented for comparison.

1) Static test (Experiment 7): This test was to evaluate the proposed MDD methods when the test phone was in static mode. Data in SET 7 was used in this test. The measurements without any interference are shown in Figure 13a as a reference. It can be noticed that as the test phone is in static mode, the 3-axis measurements are all very stable with almost no fluctuations. Compared to such reference, it can be seen that the measurements show a different level of distortions when the interference phone was approaching, in, and leaving the interference zone. The figure shows that the distortion level increases when the interference phone is close to the test phone and decreases when the interference phone is away from the test phone. Based on such reference, it can be observed from Figure 13c and 13d that the proposed two methods can well detect the magnetic disturbance even if the disturbance level is very low when the interference phone was approaching (from 5s to 8s) and leaving the interference zone (from 13s to 15s).

TABLE III
COMPARISON OF THE DETECTION ACCURACY AMONG DIFFERENT METHODS

Test	Detection accuracy using different methods				
	GMM	k-means	VSM1*	VSM2*	VSM3*
Static test	94.41%	89.83%	70.68%	74.07%	69.83%
Dynamic test	94.13%	85.77%	70.46%	80.25%	77.40%

* The threshold was set as 0.1, 0.2 and $0.3\mu T$ in VSM1, VSM2 and VSM3, respectively.

In addition, to further analyze the predicted results, statistical features of the predicted clusters were computed and compared to their true values. As shown in Table IV, the predicted values of the covariance and the average magnitude of both pure and interfered samples are very close to the true values. This illustrates that both the GMM-based MDD method and k-means-based MDD method can well cluster the unlabeled samples according to their statistical features. The clusters predicted by both methods always have similar characteristics as the true clusters.

The predicted features of each sample of both methods were also visualized in Figure 14. It can be seen from the figure that the pattern of the pure samples in Figure 14b is similar to the reference in Figure 14a, while the interfered samples show a distinct pattern. The covariance of each sample predicted by the GMM-based MDD method is marked by different colors and visualized in Figure 14c. It can be observed from the figure that the visualization of the samples' covariance is consistent with their true labels. The interfered samples are always in a lighter color than the pure samples. This indicates that the interfered samples have higher covariance than the pure samples. Similarly, different colors are used to denote the magnitude of each sample in Figure 14d. It can be observed from the figure that the pure samples usually have less magnitude than the interfered samples. The results mentioned above are consistent with the results in the preliminary experiments and analysis in Section II-B.

Additionally, to further analyze the predicted results, the statistical features of the predicted clusters were computed and compared to their true values. As shown in Table IV, the predicted values of the covariance and the average magnitude

TABLE IV
COMPARISON OF THE STATISTICAL FEATURES BETWEEN THE PREDICTIONS AND THE TRUE VALUES

Label of clusters	Static test (Experiment 7)		Dynamic test (Experiment 8)	
	Norm of covariance* (μT^2)	Magnitude in average† (μT)	Norm of covariance* (μT^2)	Magnitude in average† (μT)
Pure (true label)	0.90	50.25	13.79	47.86
Interfered (true label)	57.91	61.51	90.08	49.86
Pure (predicted label)	1.30	50.92	13.42	47.20
Interfered (predicted label)	56.87	63.70	77.22	55.60

* The covariance of each cluster with different labels predicted by GMM-based MDD method is calculated by its diagonal covariance matrix.
† The magnitude in average of each cluster with different labels predicted by k-means-based MDD method is calculated by the distance between the predicted centorid and the origin.

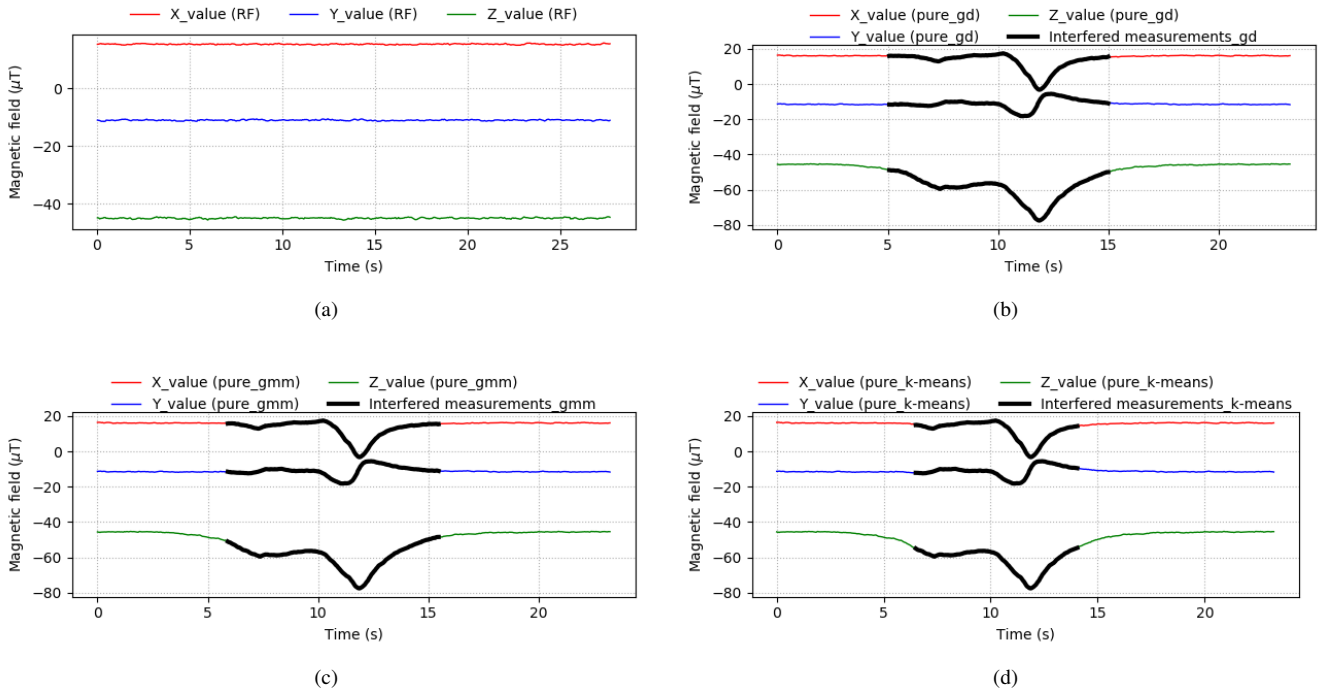

Fig. 13. 2D-visualization of the experimental results of Experiment 7: (a) reference (no interference); (b) samples with true labels; (c) samples with predicted labels using GMM-based MDD method; (d) samples with predicted labels using k-means-based MDD method.

of both pure and interfered samples are very close to the true values. This illustrates that both the GMM-based MDD method and k-means-based MDD method can well cluster the unlabeled samples according to their statistical features. The clusters predicted by both methods always have similar characteristics as the true clusters.

To quantify the performance of the proposed methods on the magnetic disturbance detection problem, the identification accuracy of the two methods were calculated and compared to the conventional vector selection method (VSM). As the results are listed in Table III, the proposed GMM-based MDD method shows the best accuracy of 94.41%. At the same time, the proposed k-means-based MDD method can also offer a good performance of nearly 90%. However, the VSM methods with different thresholds can only provide detection accuracy lower than 75%.

2) Dynamic test (Experiment 8): More critically, a dynamic situation is considered to evaluate the performance of the proposed methods against the magnetic disturbance from the infrastructures when the pedestrian holds the device using the data in SET 8. A heating radiator was used as the interference in this test. Similar to the previous test, the measurements when the volunteer was far away from the interference (heating radiator) are plotted in Figure 15a as a reference. It can be observed from the figure that some expected fluctuations are caused by pedestrian vibrations even if there is no interference. When the smartphone enters the heating radiator's interference zone, the measurements show strong distortions. The measurements tend to be stable when the smartphone leaves the heating radiator. As shown in Figure 15c and Figure 15d, the proposed GMM-based MDD method shows better performance than the k-means-based MDD method when the disturbance level is relatively low when the volunteer was approaching and leaving the interference zone (from 6s to 7s and 10.5 to 12s approximately).

Also, the true and predicted statistical features were calculated for comparison. It can be observed from Table IV that the difference between the predicted and the true

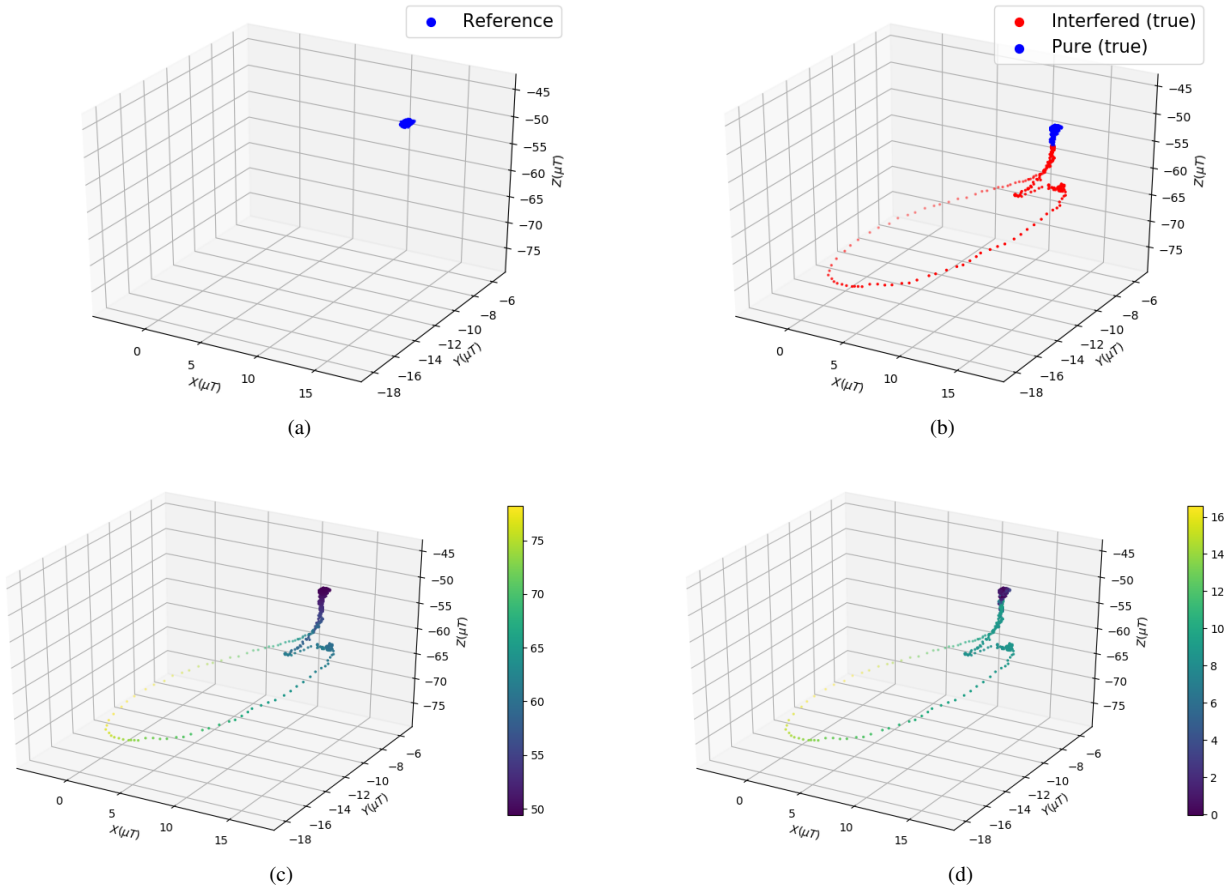

Fig. 14. 3D-visualization of the experimental results of Experiment 7: (a) reference (no interference); (b) samples with true labels; (c) samples are marked by different color according to the predicted covariance using the GMM-based MDD method; (d) samples are marked by different color according to the predicted magnitude difference using k-means-based MDD method.

statistical features of the interfered samples in dynamic mode is larger than the static mode. This is mainly caused by the smartphone's vibration when the volunteer was walking. However, such an expected prediction error caused by the vibration does not significantly degrade the proposed methods' performance.

The samples were also visualized according to the statistical features for further analysis. As it can be observed from Figure 16 that although the distributions of the pure and interfered samples in dynamic mode are much more complex than the static mode, the proposed methods can still well partition the samples into two clusters according to their covariance and magnitude. The figure again proves that the interfered samples usually have higher covariance and magnitude than the pure samples. This result is consistent with the results obtained in the previous static test and the preliminary analysis.

Similar to the previous test, the detection accuracy is calculated. As listed in Table III, the detection accuracy of the k-means-based MDD method decreases from 89.83% to 85.77%. In contrast, the GMM-based MDD method can maintain an accuracy of over 94%. The proposed methods are again compared to the conventional VSM methods. Although there are some improvements in the performance of the VSM methods, their results are still far worse than the proposed methods.

Summary: The experimental results show that both the GMM and k-means-based MDD methods can better detect magnetic disturbance than the widely adopted VSM methods in both static and dynamic modes. The experiments in this subsection again prove that the interfered samples usually have higher covariance and magnitude than the pure samples. This is consistent with our preliminary analysis in Section II-B. Moreover, it can be observed from the results that the GMM-based MDD method is more reliable than the k-means-based method in detecting a low level of disturbance. This is because the interfered and pure samples show distinct variation characteristics among the 3-axis measurements, which can be better represented by the covariance rather than the average magnitude in some cases.

However, the proposed methods show much higher computation complexity in trade of better detection performance. The time complexity of GMM and k-means-based MDD method are $O(k * n * d^3)$ and $O(k * n * d)$, respectively (k denotes the number of clusters; n is the number of total samples; d represents the dimension of each sample). While VSM methods do not need extra computation as illustrated in the literature [16].

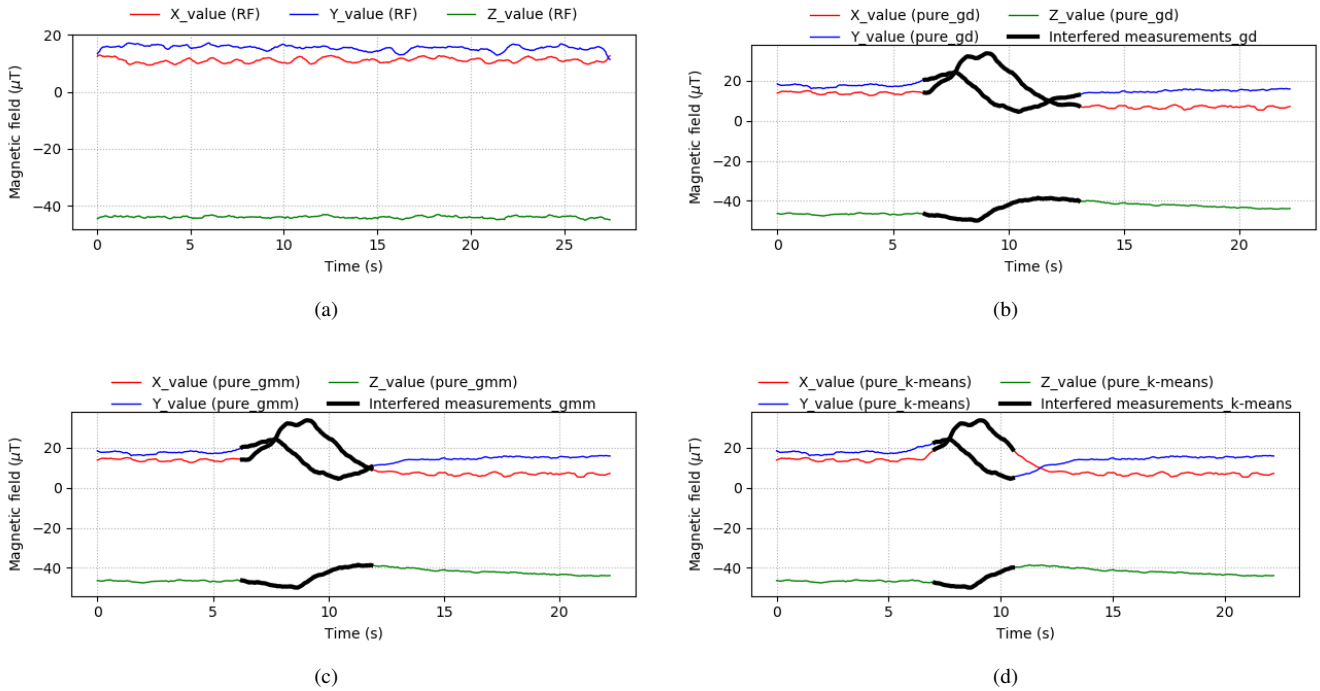

Fig. 15. Experimental results of Experiment 8: (a) reference (no interference); (b) samples with true labels; (c) samples with predicted labels using GMM-based MDD method; (d) samples with predicted labels using k-means-based MDD method.

V. Conclusion

This paper first extracted and explored the statistical features of the magnetometer measurements. Then, two unsupervised learning-based methods were proposed to detect magnetic disturbances for smartphone-based indoor positioning systems. To the best of the authors' knowledge, this paper is the first to employ unsupervised learning to tackle the magnetic disturbance detection problem. In this paper, the preliminary analysis based on extensive experiments with various experimental settings shows that the covariance and magnitude of the 3-axis measurements can help identify the magnetic disturbances. Based on this, two unsupervised learning-based magnetic disturbance detection methods using the GMM and the k-means were proposed to further explore the potential of using such two features to cluster the unlabeled samples, respectively. Unlike the widely adopted vector section methods, evaluations under critical conditions demonstrate that the proposed methods can provide outstanding detection accuracy in static and dynamic situations. Moreover, comparisons between the two proposed methods reveal that the GMM-based method is more reliable than the k-means-based method. However, in trade of better disturbance detection performance, the GMM-based MDD method shows higher computation complexity than the k-means-based MDD method. Also, the proposed methods in this study are designed for non-real-time use. This means that the methods can perform once the data have been collected. And hence the proposed methods are not suitable for some real-time applications, such as pedestrian dead reckoning or other real-time navigation applications.

The proposed methods can be integrated into various magnetometer-dominated and magnetometer-aided indoor positioning systems for different applications. It will be worth exploring the proposed methods in large crowdsourced indoor positioning systems taking into account the complex indoor environments and diverse devices (smartphones and magnetometers). One aspect of our future work is to extend the proposed algorithms to heading estimation in user trajectory construction for crowdsourced indoor positioning systems.

References

[1] B. Hofmann-Wellenhof, H. Lichtenegger, and J. Collins, *Global Positioning System: Theory and Practice*, vol. 1. Wien, Austria: Springer-Verlag, 1993.

[2] H. Falaki, R. Mahajan, S. Kandula, D. Lymberopoulos, R. Govindan, and D. Estrin, "Diversity in smartphone usage," in *Proc. 8th Int. Conf. Mobile Syst., Appl., Services*, 2010, pp. 179–194.

[3] M. Youssef and A. Agrawala, "The Horus WLAN location determination system," in *Proc. 3rd Int. Conf. Mobile Syst., Appl., Services*, 2005, pp. 205–218.

[4] C. Yao and W. Hsia, "An Indoor Positioning System Based on the Dual-Channel Passive RFID Technology," in *IEEE Sensors Journal*, vol. 18, no. 11, pp. 4654-4663, 1 June1, 2018, doi: 10.1109/JSEN.2018.2828044.

[5] I. Klein, Y. Solaz and G. Ohayon, "Pedestrian Dead Reckoning With Smartphone Mode Recognition," in *IEEE Sensors Journal*, vol. 18, no. 18, pp. 7577-7584, 15 Sept.15, 2018, doi: 10.1109/JSEN.2018.2861395.

[6] R. Shirai and M. Hashimoto, "DC Magnetic Field Based 3D Localization With Single Anchor Coil," in *IEEE Sensors Journal*, vol. 20, no. 7, pp. 3902-3913, 1 April1, 2020, doi: 10.1109/JSEN.2019.2961365.

[7] V. Pasku, A. D. Angelis, G. D. Angelis, D. D. Arumugam, M. Dionigi, P. Carbone, A. Moschitta, and D. S. Ricketts, "Magnetic field-based positioning systems," *IEEE Commun. Surveys Tuts.*, vol. 19, no. 3, pp. 2003–2017, Mar. 2017.

[8] K. P. Subbu, B. Gozick, and R. Dantu, "LocateMe: Magnetic-fieldsbased indoor localization using smartphones," *ACM Trans. Intell. Syst. Technol.*, vol. 4, no. 4, 2013, Art. no. 73.

[9] Y. Shu, C. Bo, G. Shen, C. Zhao, L. Li, and F. Zhao, "Magicol: Indoor localization using pervasive magnetic field and opportunistic WiFi sensing," *IEEE J. Sel. Areas Commun.*, vol. 33, no. 7, Jul. 2015.

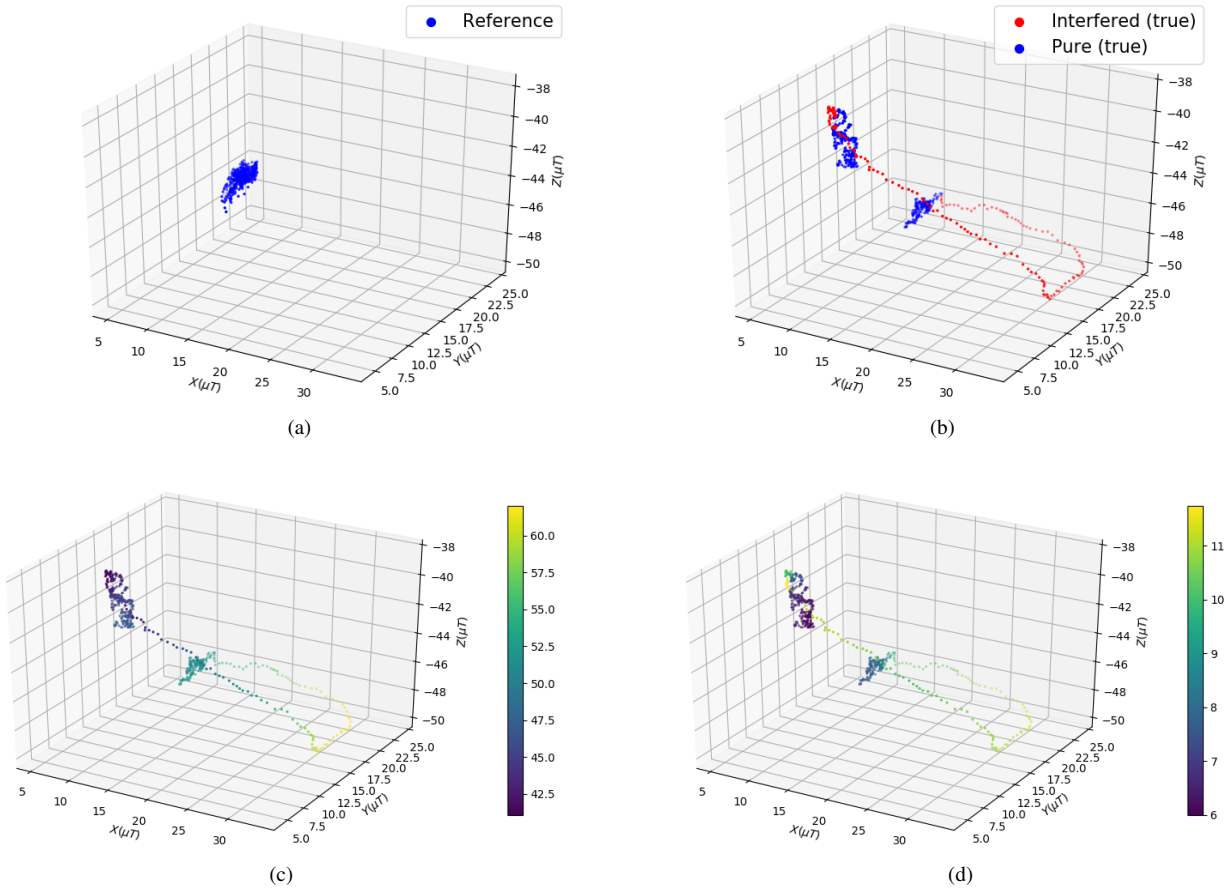

Fig. 16. 3D-visualization of the experimental results of Experiment 8: (a) reference (no interference); (b) samples with true labels; (c) samples are marked by different color according to the predicted covariance using the GMM-based MDD method; (d) samples are marked by different color according to the predicted magnitude difference using k-means-based MDD method.

[10] I. Ashraf, S. Hur, S. Park, and Y. Park, "DeepLocate: Smartphone based indoor localization with a deep neural network ensemble classifier," *Sensors*, vol. 20, no. 1, p. 133, 2020

[11] I. Ashraf, Y. B. Zikria, S. Hur and Y. Park, "A Comprehensive Analysis of Magnetic Field Based Indoor Positioning With Smartphones: Opportunities, Challenges and Practical Limitations," in *IEEE Access*, vol. 8, pp. 228548-228571, 2020, doi: 10.1109/ACCESS.2020.3046288.

[12] A. Rai, K. K. Chintalapudi, V. N. Padmanabhan, and R. Sen, "Zee: Zero-effort crowdsourcing for indoor localization," in *Proc. 18th Annu. Int. Conf. Mobile Comput. Netw.*, 2012, pp. 293–304.

[13] V. Radu and M. Marina, "HiMLoc: Indoor smartphone localization via activity aware pedestrian dead reckoning with selective crowdsourced WiFi fingerprinting," in *Proc. Int. Conf. Indoor Positioning Indoor Navigat.*, Oct. 2013, pp. 1–10.

[14] W. Zhao, S. Han, R. Q. Hu, W. Meng and Z. Jia, "Crowdsourcing and Multisource Fusion-Based Fingerprint Sensing in Smartphone Localization," in *IEEE Sensors Journal*, vol. 18, no. 8, pp. 3236-3247, 15 April15, 2018, doi: 10.1109/JSEN.2018.2805335.

[15] Y. Wu, D. Zou, P. Liu and W. Yu, "Dynamic Magnetometer Calibration and Alignment to Inertial Sensors by Kalman Filtering," in *IEEE Transactions on Control Systems Technology*, vol. 26, no. 2, pp. 716-723, March 2018, doi: 10.1109/TCST.2017.2670527.

[16] B. Fan, Q. Li, and T. Liu, "How magnetic disturbance influences the attitude and heading in magnetic and inertial sensor-based orientation estimation," *Sensors*, vol. 18, no. 1, p. 76, 2018.

[17] Z. Zhang, X. Meng and J. Wu, "Quaternion-Based Kalman Filter With Vector Selection for Accurate Orientation Tracking," in *IEEE Transactions on Instrumentation and Measurement*, vol. 61, no. 10, pp. 2817-2824, Oct. 2012, doi: 10.1109/TIM.2012.2196397.

[18] N. Yadav and C. Bleakley, "Accurate orientation estimation using AHRS under conditions of magnetic distortion," Sensors, vol. 14, no. 11, pp. 20008–20024, Jan. 2014.

[19] B. Fan, Q. Li, C. Wang, and T. Liu, "An adaptive orientation estimation method for magnetic and inertial sensors in the presence of magnetic disturbances," *Sensors*, vol. 17, no. 6, p. 1161, Mar. 2017.

[20] W. Youn, M. B. Rhudy, A. Cho and H. Myung, "Fuzzy Adaptive Attitude Estimation for a Fixed-Wing UAV With a Virtual SSA Sensor During a GPS Outage," in *IEEE Sensors Journal*, vol. 20, no. 3, pp. 1456-1472, 1 Feb.1, 2020, doi: 10.1109/JSEN.2019.2947489.

[21] G. Ligorio and A. M. Sabatini, "Dealing with magnetic disturbances in human motion capture: A survey of techniques," *Micromachines*, vol. 7, no. 3, p. 43, Mar. 2016.

[22] D. Roetenberg, H. J. Luinge, C. T. M. Baten and P. H. Veltink, "Compensation of magnetic disturbances improves inertial and magnetic sensing of human body segment orientation," in *IEEE Transactions on Neural Systems and Rehabilitation Engineering*, vol. 13, no. 3, pp. 395-405, Sept. 2005, doi: 10.1109/TNSRE.2005.847353.

[23] W. Qi, H. Su and A. Aliverti, "A Smartphone-Based Adaptive Recognition and Real-Time Monitoring System for Human Activities," in *IEEE Transactions on Human-Machine Systems*, vol. 50, no. 5, pp. 414-423, Oct. 2020, doi: 10.1109/THMS.2020.2984181.

[24] Y. Hsu, J. Wang and C. Chang, "A Wearable Inertial Pedestrian Navigation System With Quaternion-Based Extended Kalman Filter for Pedestrian Localization," in *IEEE Sensors Journal*, vol. 17, no. 10, pp. 3193-3206, 15 May15, 2017, doi: 10.1109/JSEN.2017.2679138.

[25] D. A. Reynolds. Gaussian mixture models. pages 659–663,2009.

[26] Hartigan, J. A. and Wong, M. A. (1979). Algorithm as 136: A k-means clustering algorithm. *Journal of the royal statistical society. series c (applied statistics)*, 28(1):100– 108.